Journal of the Optical Society of Korea, Vol. 10, No. 4, December 2006, pp. 188-195

Third-Harmonic Generation Microscopy for Material Characterization

Arnaud Royon[1,2]*

[1]*CPMOH-CNRS, Univ. of Bordeaux 1, 351 Cours de la Libération, 33405 Talence cedex, France*
[2]*College of Optics and Photonics/CREOL, UCF, 4000 Central Florida Blvd. Orlando, Florida, 32816, USA*

Bruno Bousquet and Lionel Canioni

CPMOH-CNRS, Univ. of Bordeaux 1, 351 Cours de la Libération, 33405 Talence cedex, France

Mona Treguer, Thierry Cardinal, and Evelyne Fargin

ICMCB-CNRS, Univ. of Bordeaux 1, 87 Avenue du Docteur Schweitzer, 33608 Pessac cedex, France

Dae-Geun Kim and Seung-Han Park

National Research Laboratory of Nonlinear Optics, Yonsei University, Seou 120-749l, Korea

(Received December 15, 2006 : revised December 20, 2006)

Third harmonic generation microscopy is described in the frame work of the theory of harmonic generation with Gaussian focused beams inside a bulk material as well as at the vicinity of an interface. This model is then applied to characterize different types of materials in terms of electronic third-order susceptibility. Examples of bulk glasses, poled glasses, laser-induced modifications in glasses and nanoparticles in solution are given in order to give a survey of the broad application field of THG microscopy in material characterization.

OCIS codes : 180.0180, 190.0190, 190.4180, 300.6420

I. INTRODUCTION

Third-Harmonic Generation (THG) is a coherent third-order nonlinear process related to the third-order susceptibility $x^{(3)}(-3\omega;\omega,\omega,\omega)=x^{(3)}$ that mixes three photons at the optical angular frequency ω to generate a photon at three times the angular frequency of the incident photons, *i.e.* 3ω. This effect has mainly been studied to convert visible laser light into UV radiation [1]. Nevertheless, its low conversion efficiency is an obstacle for direct laser frequency tripling and cascading second-order processes (second-harmonic generation and sum-frequency generation) have been preferred to achieve this goal [2]. THG has also been studied to measure the third-order susceptibility $x^{(3)}$ of different materials, especially glasses, because they show a wide transparent region permitting the fundamental and the third-harmonic beams not being absorbed [3-6]. Although THG is an inefficient process in a bulk material in which the phase mismatch condition is not suitable, it becomes appreciable at the vicinity of an interface [7] where a discontinuity in the refractive indices and/or the third-order susceptibilities is present. When a fundamental laser beam is focused near an interface, a coherent third-harmonic beam is generated allowing the imaging of interfaces of any material. The first nonlinear scanning laser THG microscope was built in 1997 [8]. This technique has since spread and has been used for non-invasive biological imaging [9-12] and for $x^{(3)}$ measurements in thin films [13-14] and solutions [15].

In this paper, a theoretical approach of the THG with focused Gaussian beams in a bulk material as well as near an interface is given [16-18]. Different applications of this technique for the characterization of materials are then proposed and their corresponding experimental results are shown.

II. THEORY

Let us consider an incident monochromatic linearly polarized beam at the angular frequency ω propagating

in the positive z-direction (direct wave) which electric field is of the form:

$$\vec{E}_{\omega}(\vec{r};t)=\frac{1}{2}\left\{\vec{A}_{\omega}(\vec{r})\exp[i(k_{\omega}z-\omega t)]+\vec{A}^{*}_{\omega}(\vec{r})\exp[-i(k_{\omega}z-\omega t)]\right\} \quad (1)$$

This electric field induces a third-order nonlinear polarization, which is the sum of two different contributions, one at the angular frequency ω, responsible of the optical Kerr effect and one at the angular frequency 3ω, responsible of the third-harmonic generation process. This last contribution is given by:

$$\vec{P}_{3\omega}=\frac{1}{2}\left\{\vec{p}_{3\omega}\exp[i(3k_{\omega}z-3\omega t)]+\vec{p}^{*}_{3\omega}\exp[-i(3k_{\omega}z-3\omega t)]\right\} \quad (2)$$

where

$$\vec{p}_{3\omega}=\frac{1}{4}\varepsilon_0\chi^{(3)}\vec{A}^{3}_{\omega} \quad (3)$$

Starting from the nonlinear wave equation and assuming that the amplitude of the fundamental electric field does not vary too much on a distance of a wavelength (slowly variable amplitude approximation), one can obtain the paraxial wave equation for the third-harmonic electric field:

$$\nabla^2_{\perp}\vec{A}_{3\omega}+2ik_{3\omega}\frac{\partial\vec{A}_{3\omega}}{\partial z}=-\mu_0(3\omega)^2\vec{p}_{3\omega}\exp(i\Delta kz) \quad (4)$$

where $\nabla^2_{\perp}$ is the transverse Laplacian, $\triangle k = 3k_{\omega} - k_{3\omega}$ the phase mismatch between the fundamental wave and the third-harmonic wave, $k_{\omega}=n_{\omega}\frac{\omega}{c}$ the wave vector of the fundamental beam and $k_{3\omega}=n_{3\omega}\frac{3\omega}{c}$ the wave vector of the third-harmonic beam.

The use of a laser applies to work with Gaussian beams so that the expressions of the fundamental and third-harmonic electric fields are given by:

$$A_{\omega}(\rho;z)=\frac{A_{0\_\omega}}{1+i\xi}\exp\left[\frac{-\rho^2}{w_0^2(1+i\xi)}\right] \quad (5)$$

$$A_{3\omega}(\rho;z)=\frac{A_{0\_3\omega}(z)}{1+i\xi}\exp\left[\frac{-3\rho^2}{w_0^2(1+i\xi)}\right] \quad (6)$$

where $\rho=\sqrt{x^2+y^2}$ is the radial coordinate, $\xi=\frac{z}{z_R}=\frac{2z}{b}$ a longitudinal coordinate defined in terms of confocal parameter $b=2z_R=\frac{2\pi w_0^2}{\lambda}=kw_0^2$ and w_0 the beam waist of the fundamental wave.

Substituting these expressions in the paraxial equation gives the following differential equation, which translates the evolution of the amplitude of the third-harmonic electric field with respect to the distance z:

$$\frac{dA_{0\_3\omega}(z)}{dz}=i\frac{3\omega}{8n_{3\omega}c}\chi^{(3)}A^3_{0\_\omega}\frac{\exp(i\Delta kz)}{(1+i\xi)^2} \quad (7)$$

The solution of this equation is:

$$A_{0\_3\omega}(z)=i\frac{3\omega}{8n_{3\omega}c}A^3_{0\_\omega}\chi^{(3)}J_{3\omega}(\Delta k;z_0;z) \quad (8)$$

where $J_{3\omega}(\triangle k;\, z_0;\, z)=\int_{z_0}^{z}\frac{\exp(i\triangle ku)}{\left(1+\frac{2iu}{b}\right)^2}du$ is the third-harmonic interaction length and z_0 the position of the entrance of the medium; the position of the beam waist is set to be at $z=0$.

This third-harmonic interaction length can be evaluated analytically in two particular cases.

The first case corresponds to a slightly focused beam (plane wave limit), for which and

$$\left|J_{3\omega}(\Delta k;z_0;z)\right|^2=\left|\int_{z_0}^{z}\exp(i\Delta ku)du\right|^2=\left|\frac{\exp(i\Delta kz)-\exp(i\Delta kz_0)}{i\Delta k}\right|^2$$
$$=L^2\mathrm{sinc}^2\left(\frac{\Delta kL}{2}\right) \quad (9)$$

In this plane wave limit, the usual phase matching behavior is found.

The second case corresponds to a strongly focused beam inside the medium, for which $z_0=-|z_0|$, $z=|z|$ and $b<<|z_0|$ et $|z|$ and the third-harmonic interaction length can be evaluated by a contour integral:

$$J_{3\omega}(\Delta k;z_0;z)=\int_{-\infty}^{+\infty}\frac{\exp(i\Delta ku)}{\left(1+\frac{2iu}{b}\right)^2}du=\begin{cases}0 \text{ if } \Delta k\le 0\\ \pi\frac{b^2}{2}\Delta k\exp\left(-\frac{b\Delta k}{2}\right) \text{ if } \Delta k>0\end{cases} \quad (10)$$

Finally, the third-harmonic irradiance generated in a bulk material and detected in the far-field is given by:

$$I_{3\omega}=\left(\frac{3\omega}{4\varepsilon_0c^2}\right)^2\frac{1}{n_{3\omega}n^3_{\omega}}I^3_{\omega}\left|\chi^{(3)}J_{3\omega}(\Delta k;z_0;z)\right|^2 \quad (11)$$

From equation (10), one can notice that the third-harmonic interaction length is null when $\triangle k\le 0$, which is the case for all the materials that have a normal dispersion in the wavelength range of interest ($\lambda/3 \rightarrow \lambda$). As a result, the third-harmonic irradiance is zero in the far-field when the incident fundamental laser beam is focused inside a medium. This is known as the

Gouy phase shift anomaly. Nevertheless, if the fundamental beam is focused at the vicinity of an interface separating two media of different refractive indices and/or third-order susceptibilities, an appreciable third-harmonic beam can be detected in the far-field even if the media have a negative or null phase mismatch. If the interface separates two infinite media with different refractive indices n_i and different third-order susceptibilities $x_i^{(3)}$ ($i = 1$ or 2) with the interface at $z = 0$, the third-harmonic irradiance in the far-field is:

$$I_{3\omega} = \left(\frac{3\omega}{4\varepsilon_0 c^2}\right)^2 I_\omega^3 \left| \frac{n_{\omega,1}^{3/2}}{n_{3\omega,1}} \chi_1^{(3)} J_{3\omega,1}(\Delta k_1;-\infty;0) + \frac{n_{\omega,2}^{3/2}}{n_{3\omega,2}} \chi_2^{(3)} J_{3\omega,2}(\Delta k_2;0;+\infty) \right|^2 \tag{12}$$

Although equation (12) appears complicated, it can be simplified in two particular cases [18].

The first case is an interface air/semi-infinite material. The third-order susceptibility of air ($\sim 10^{-25}$ $m^2.V^{-2}$) is negligible compared to that of the material. The third-harmonic irradiance is therefore given by:

$$I_{3\omega} = \left(\frac{3\omega}{4\varepsilon_0 c^2}\right)^2 I_\omega^3 \left| \frac{n_{\omega,2}^{3/2}}{n_{3\omega,2}} \chi_2^{(3)} J_{3\omega,2}(\Delta k_2;0;+\infty) \right|^2 \tag{13}$$

The second case is an interface separating two media presenting identical refractive indices and different third-order susceptibilities. This implies the following relations: $n_{\omega,1} = n_{\omega,2} = n_\omega$, $n_{3\omega,1} = n_{3\omega,2} = n_{3\omega}$, $\triangle k_1 = \triangle k_2 = \triangle k$ and $J_{3\omega,1}(\triangle k_1;-\infty;0) = -J_{3\omega,2}(\triangle k_2;0;+\infty)$. The third-harmonic irradiance is therefore given by:

$$I_{3\omega} = \left(\frac{3\omega}{4\varepsilon_0 c^2}\right)^2 I_\omega^3 \frac{n_\omega^3}{n_{3\omega}^2} \left| J_{3\omega,1}(\Delta k;-\infty;0) \right|^2 \left| \chi_1^{(3)} - \chi_2^{(3)} \right|^2 \tag{14}$$

Now, let us assume an incident circularly polarized electric field of the form:

$$\vec{E}_\omega(\vec{r};t) = \frac{1}{2}(\vec{e}_x + i\vec{e}_y)\{A_\omega(\vec{r})\exp[i(k_\omega z - \omega t)] + A_\omega^*(\vec{r})\exp[-i(k_\omega z - \omega t)]\} \tag{15}$$

Considering an isotropic material, the Kleinman symmetry conditions show that the third-order susceptibility tensor presents 21 nonzero elements of which only 3 are independent. They are [17]:

$$\begin{aligned} &xxxx = yyyy = zzzz \\ &yyzz = zzyy = zzxx = xxzz = xxyy = yyxx = \frac{\sigma}{3} \\ &yzyz = zyzy = zxzx = xzxz = xyxy = yxyx = \frac{\sigma}{3} \\ &yzzy = zyyz = zxxz = xzzx = xyyx = yxxy = \frac{\sigma}{3} \\ &xxxx = xxyy + xyxy + xyyx = \sigma \end{aligned} \tag{16}$$

The third-order nonlinear polarization induced in the material is then:

$$\begin{aligned} \vec{P}(\vec{r};\omega) &= \varepsilon_0 \chi^{(3)}(\omega)\vec{E}(\vec{r};\omega)\vec{E}(\vec{r};\omega)\vec{E}(\vec{r};\omega) \\ \vec{P}(\vec{r};\omega) &= \varepsilon_0 \begin{bmatrix} -\frac{2}{3}\sigma + \left(\sigma - \frac{\sigma}{3}\right) \\ \frac{2}{3}\sigma + \left(\frac{\sigma}{3} - \sigma\right) \\ 0 \end{bmatrix} \begin{bmatrix} E_x(\vec{r};\omega) \\ iE_y(\vec{r};\omega) \\ 0 \end{bmatrix} = \begin{bmatrix} 0 \\ 0 \\ 0 \end{bmatrix} \end{aligned} \tag{17}$$

From equation (17), it appears that the third-order nonlinear polarization induced by a circularly polarized electric field is null; no third harmonic can be generated with such a polarization. Nevertheless, if the material presents a crystalline structure, the third-order nonlinear polarization is no longer null and THG can occur if the beam is focused at the vicinity of an interface. Hence, by changing the polarization of the incident beam, structural information of the studied material can be obtained [19-20].

III. EXPERIMENT

Two different experimental setups with different laser sources have been used. The generic experimental setup is shown in fig. 1 and the geometry of the experiment with focused Gaussian beams at the vicinity of an interface separating two media is given in fig. 2.

The first setup uses an optical parametric oscillator (Spectra-Physics, Tsunami-Opal system) which delivers 130 fs pulses at the wavelength of 1500 nm at the repetition rate of 80 MHz [13]. The laser beam is focused on the sample with a microscope objective (working distance = 700 μm; NA = 0.65). The third-harmonic beam is collected with a condenser (working distance = 3 cm; NA = 0.6), filtered from the fundamental wavelength using an interference filter (λ_0 = 500 nm; $\Delta\lambda$ = 40 nm) and measured with a photomultiplier tube (PMT, Hammamatsu R5700). The photocurrent from the PMT is amplified and synchronously detected with a mechanical chopper via a lock-in amplifier, digitized and sent to a computer for acquisition. An x-y-scan can be realized with a piezoelectric translation stage as well as galvanometric mirrors and the z-scan is carried out with a piezoelectric translation stage.

The second setup uses an oscillator (Amplitude Systemes, t-Pulse) which delivers 200 fs pulses at the wavelength of 1030 nm at the repetition rate of 50

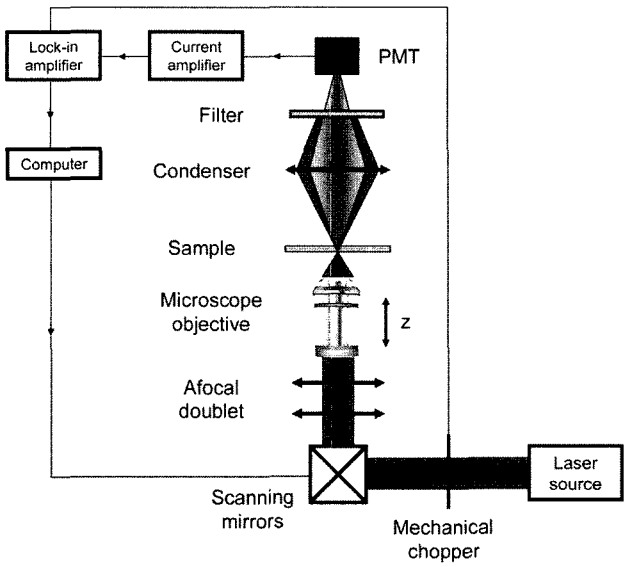

FIG. 1. Generic experimental setup.

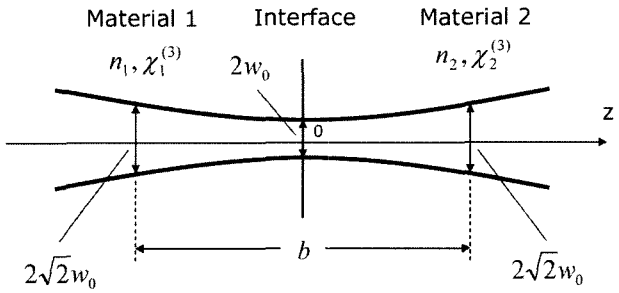

FIG. 2. Geometry of the experiment with a focused Gaussian beam at the vicinity of an interface separating two media with different optical properties.

MHz. The laser beam is focused on the sample with a microscope objective (working distance = 500 μm; NA = 0.7). The third-harmonic beam is collected with a condenser (working distance = 3 cm; NA = 0.6), filtered from the fundamental wavelength using an interference filter (λ_0 = 343 nm; $\Delta\lambda$ = 40 nm) and measured with a photomultiplier tube (PMT, Hammamatsu R5700). The photocurrent from the PMT is amplified, digitized and sent to a computer for acquisition. An x-y-scan can be realized in less than 2s with two galvanometric mirrors and the z-scan is carried out with the motor of a modified Zeiss Axiovert 200 M microscope.

IV. EXPERIMENTAL RESULTS

4.1 $x^{(3)}$ measurements in bulk materials

The THG experiments have been carried out with the OPO source, on 300 μm-thick phosphate and borophosphate glass matrices containing niobium oxide at different concentrations [21-22]. The measurements have been calibrated with respect to a fused silica sample with a similar thickness. The THG signal has been measured for the beam waist at the vicinity of the first interface (*i.e.* air/glass interface) to get the best point of focus; moreover, it should be noted that the third harmonic is not absorbed because the absorption coefficient is low at 500 nm. Indeed, no absorption could be measured using a standard spectrophotometer with 1 mm-thick samples. Fresnel transmission and refractive index dispersion corrections have been performed. Since no significant two-photon absorption occurs at this wavelength, the imaginary part of the electronic susceptibility has been neglected and the calculated modulus of the susceptibility was set to the real part. Finally, the electronic susceptibility is given by:

$$\chi^{(3)}_{1111} = \sqrt{\frac{T^3_{3\omega,SiO_2} T^3_{\omega,SiO_2}}{T_{3\omega} T^3_{\omega}}} \sqrt{\frac{I_{3\omega}}{I_{3\omega,SiO_2}}} \sqrt{\frac{n_{3\omega} n^3_{\omega}}{n_{3\omega,SiO_2} n^3_{\omega,SiO_2}}} \left| \frac{J_{3\omega,SiO_2}(\Delta k_{SiO_2}; 0; L_{SiO_2})}{J_{3\omega}(\Delta k; 0; L)} \right| \chi^{(3)}_{1111,SiO_2} \quad (18)$$

where T_ω, n_ω, $T_{3\omega}$, $n_{3\omega}$ are the Fresnel transmission coefficients and the refractive indices at ω and 3ω, respectively, $I_{3\omega}$ the detected third-harmonic irradiance, $J_{3\omega}(\Delta k; 0; L) = \int_0^L \frac{\exp(i\Delta k u)}{\left(1+\frac{2iu}{b}\right)^2} du$ the third-harmonic interaction length, $\Delta k = 3k_\omega - k_{3\omega}$ the phase mismatch, $b = \pi w_0^2/\lambda$ the confocal parameter, w_0 the beam waist and L the sample thickness. The SiO_2 subscript refers to fused silica and no subscript alludes to the investigated glass.

These measurements are not straightforward because the refractive index of the investigated material at ω and 3ω frequency and the $x^{(3)}$ value of a reference material must be provided. The error measurements on the absolute value come essentially from the $x^{(3)}$ reference value. Relative measurements are preferred as they permit direct comparison between samples with a relative error of 10%. The obtained values of $x^{(3)}_{1111}$ for all samples, relative to fused silica, are reported in fig. 3. As previously observed [22], the nonlinearity increases when the niobium concentration increases in the glass network. In the present case, $x^{(3)}_{1111}$ is linear with the niobium concentration. This effect is directly related to the measurement of the electronic contribution to the nonlinearity which results in a summation of the Nb-O bonds electronic contribution.

4.2 $x^{(3)}$ measurements in poled glasses

Thermal poling is a technique which consists in applying a direct-current (dc) electric field below the glass transition temperature and then cooling the glass before removing the dc bias. Amorphous materials such

as glasses have an inversion symmetry which excludes the occurrence of second-order nonlinearities (*i.e.* $x^{(2)} \equiv 0$). After thermal poling, the coupling between the dc electric field induced inside the glass and the third-order susceptibility of the glass generates an effective $x^{(2)}$, allowing the occurrence of second-order nonlinear processes such as second-harmonic generation. Thermal poling has been carried out on borophosphate glasses containing 40% of niobium oxide with different dc electric field application times. All the experimental parameters are given by Malakho *et al.* [23].

The THG experiments have been performed with the same setup as previously on the poled regions under the surface of the glasses under study. The thickness of the poled regions and of the glasses is about 8 μm and 300 μm, respectively. The measurements have been calibrated with respect to a fused silica sample with a similar thickness (*i.e.* 300 μm). Here again, the THG signal has been measured for the beam waist at the vicinity of the first interface (*i.e.* air/poled region interface) to get the best point of focus. However, part or the third-harmonic is absorbed by the poled region, since its absorption coefficient is not zero at 500 nm. So, absorption corrections as well as Fresnel transmission and refractive index dispersion corrections have been performed. Since no significant two-photon absorption occurs at this wavelength, the imaginary part of the electronic susceptibility has been neglected and the calculated modulus of the susceptibility was set to the real part. Finally, the electronic susceptibility is given by:

$$\chi^{(3)}_{1111} = \sqrt{\frac{T_{3\omega,SiO_2} T^3_{\omega,SiO_2}}{T_{3\omega} T^3_{\omega}}} \sqrt{\frac{I_{3\omega}}{I_{3\omega,SiO_2}}} \sqrt{\frac{n_{3\omega} n^3_{\omega}}{n_{3\omega,SiO_2} n^3_{\omega,SiO_2}}} \left| \frac{J_{3\omega,SiO_2}(\Delta k_{SiO_2}; 0; L_{SiO_2})}{J_{3\omega}(\Delta k; 0; L)} \right| \exp(\alpha_{3\omega} L) \chi^{(3)}_{1111,SiO_2} \tag{19}$$

Where $a_{3\omega}$ is the absorption coefficient of the poled region at 3ω. The obtained values of $x^{(3)}_{1111}$ for the poled glasses, relative to fused silica, are reported in fig. 4. The nonlinear response increases with the poling time. This evolution has to be related with the progressive depletion of sodium ions within the poling zone inducing structural changes of the glass network [23].

4.3 $x^{(3)}$ measurements in structures inside a bulk material

The THG experiments have been carried out with the t-Pulse source, on femtosecond laser irradiation induced defects in fused silica [24]. The defects are approximately 400 μm under the surface and they are 200 μm-thick. The fused silica sample is 1 mm-thick. The irradiation pulse energy is 5 μJ and all the other experimental parameters are given by Zoubir *et al.* [24]. A z-scan of the third-harmonic signal emitted by this sample is shown in fig. 5. The third-harmonic irradiances generated at the interfaces air/silica and silica/defect, respectively, are given by:

$$I_{3\omega,air/SiO_2} = \left(\frac{3\omega}{4\varepsilon_0 c^2}\right)^2 I^3_{\omega} \frac{n^3_{\omega,SiO_2}}{n_{3\omega,SiO_2}} \times \left| \begin{array}{l} J_{3\omega,SiO_2}(\Delta k_{SiO_2}; z_0 = 0; z_1 = 400\,\mu m)\chi^{(3)}_{SiO_2} \\ + J_{3\omega,def}(\Delta k_{def}; z_1 = 400\,\mu m; z_2 = 600\,\mu m)\chi^{(3)}_{def} \\ + J_{3\omega,SiO_2}(\Delta k_{SiO_2}; z_2 = 600\,\mu m; z_3 = 1000\,\mu m)\chi^{(3)}_{SiO_2} \end{array} \right|^2 \tag{20}$$

$$I_{3\omega,SiO_2/def} = \left(\frac{3\omega}{4\varepsilon_0 c^2}\right)^2 I^3_{\omega} \frac{n^3_{\omega,def}}{n_{3\omega,def}} \times \left| \begin{array}{l} J_{3\omega,SiO_2}(\Delta k_{SiO_2}; z_0 = -400\,\mu m; z_1 = 0)\chi^{(3)}_{SiO_2} \\ + J_{3\omega,def}(\Delta k_{def}; z_1 = 0; z_2 = 200\,\mu m)\chi^{(3)}_{def} \\ + J_{3\omega,SiO_2}(\Delta k_{SiO_2}; z_2 = 200\,\mu m; z_3 = 600\,\mu m)\chi^{(3)}_{SiO_2} \end{array} \right|^2 \tag{21}$$

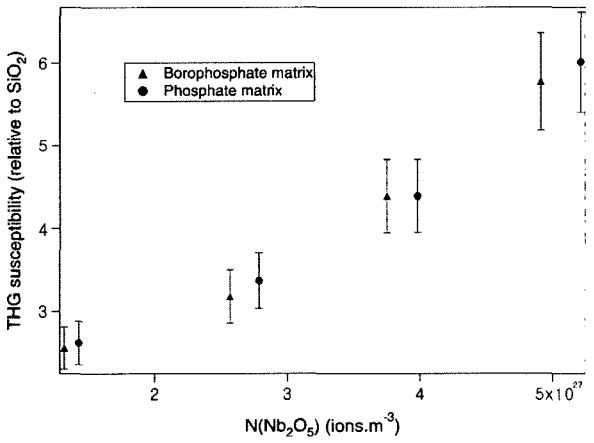

FIG. 3. THG susceptibility $x^{(3)}_{1111}$ relative to fused silica versus Nb_2O_5 concentration of the phosphate and borophosphate matrix glasses.

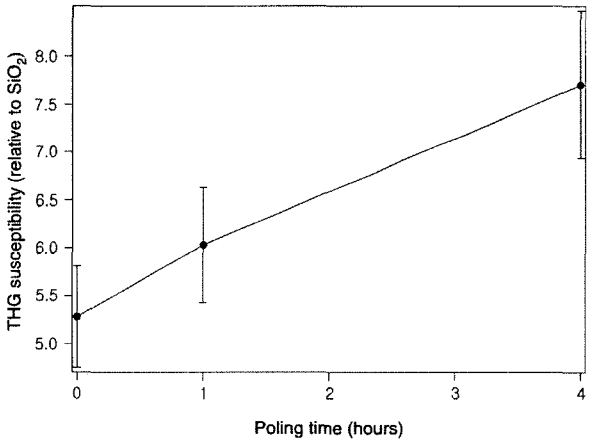

FIG. 4. THG susceptibility $x^{(3)}_{1111}$ relative to fused silica versus the dc electric field application time of the poled region of a borophosphate glass containing 40% of niobium oxide.

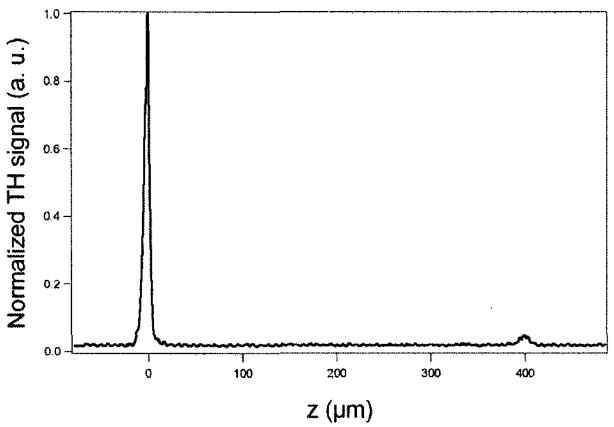

FIG. 5. Evolution of the normalized third-harmonic signal versus the z-position of a fused silica (Herasil) sample in which defects have been created by femtosecond laser irradiation. The first peak corresponds to the air/silica interface and the second peak corresponds to the silica/defects interface. The other interfaces could not be reached because of the limited working distance of the microscope objective.

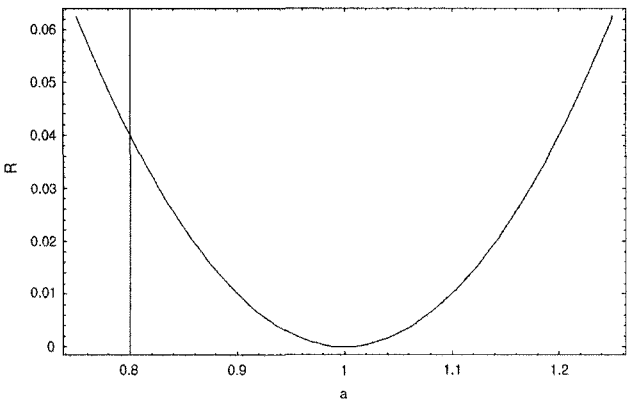

FIG. 6. Evolution of the ratio of the third-harmonic irradiances $R=\frac{I_{3\omega,SiO_2/def}}{I_{3\omega,air/SiO_2}}$ versus the ratio of the third-order susceptibilities $a=\frac{x^{(3)}_{def}}{x^{(3)}_{SiO_2}}$.

Where the SiO_2 subscript refers to fused silica and the def subscript alludes to the defect. No absorption corrections have been performed since the fused silica and the defect are transparent at both the fundamental and third-harmonic wavelengths. The refractive indices of the defect at ω and 3ω have been set to a value higher of an amount of 10^{-3} relative to the refractive indices of fused silica. This assumption is based on refractive index variation measurement of waveguides written in fused silica; at 633 nm, this variation has been measured to be about 10^{-3} [24]. By plotting the theoretical ratio $R=\frac{I_{3\omega,SiO_2/def}}{I_{3\omega,air/SiO_2}}$ versus the ratio of the third-order susceptibilities $a=\frac{x^{(3)}_{def}}{x^{(3)}_{SiO_2}}$ (cf. fig. 6) and by reporting on this graph the experimental ratio R measured in fig. 5, one can deduce the variation of the third-order susceptibility of the defect relative to fused silica. Nevertheless, by reporting one value of R, two values of a can be determined, one lower and one higher than 1. A previous experiment on the same defect, but at the surface of the material, permitted to observe a third-harmonic signal less important at the interface air/defect than at the interface air/silica and to conclude to a third-order susceptibility lower for the defect than for fused silica [24].

For a measured ratio $R\approx 0.053$, two values of a are found: 0.77 and 1.23. The value lower than 1 is retained, *i.e.* 0.77, and the variation of the third-order susceptibility of the defect relative to fused silica is:

$$\frac{\Delta\chi^{(3)}}{\chi^{(3)}}=\frac{\chi^{(3)}_{def}-\chi^{(3)}_{SiO_2}}{\chi^{(3)}_{SiO_2}}\times 100\approx -23\% \qquad (22)$$

The THG microscopy is the only technique which permits the direct measurement of the electronic third-order susceptibility of a structure embedded in a bulk material if the refractive indices at ω and 3ω of both the non-irradiated material and the defect are known. Another method to estimate the nonlinear refractive index is based on spectral broadening measurement induced by self-phase modulation of a laser pulse propagating in a waveguide [24-25]. Nevertheless, this technique does not allow a precise measurement since it relies on accurate knowledge of the pulse temporal amplitude and phase.

4.4 Comparison of the $x^{(3)}$ of different solutions

The THG experiments have been performed with the OPO source on drops, deposited on a microscope slide, of solutions containing CdS and CdS@Ag_n nanoparticles, at 3.10^{-4} and 10^{-4} mol.L-1 concentration, respectively [26]. A z-scan of the third-harmonic signal emitted by these samples is shown in fig. 7. The signal collected at the solution/air interface is given by:

$$S_{3\omega}\propto T_{3\omega,sol}T^3_{\omega,sol}\left|\frac{n^{3/2}_{\omega,sol}}{n_{3\omega,sol}}J_{3\omega,sol}(\Delta k_{sol};-L_{sol};0)\chi^{(3)}_{1111,sol}\right|^2 \qquad (23)$$

From which the third-order susceptibility can be extracted:

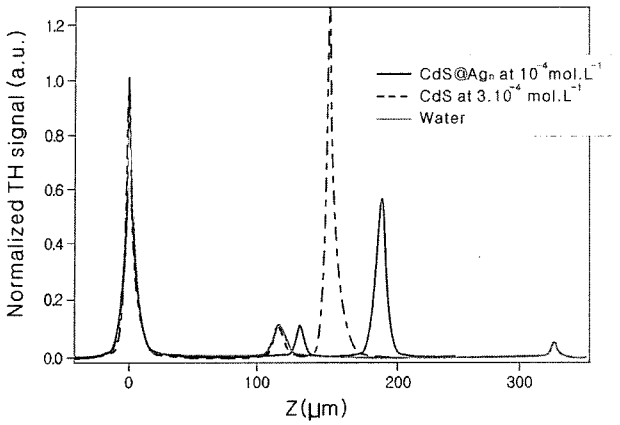

FIG. 7. Evolution of the normalized third-harmonic signal versus the z-position of three different solutions deposited on a 120 μm-thick microscope slide: a solution of CdS@Ag$_n$ at 10^{-4} mol.L^{-1}, a solution of CdS at 3.10^{-4} mol.L^{-1} and some water for comparison. The first right peak corresponds to the air/slide interface, the second to the slide/solution interface and the third to the solution/air interface. The thickness of the drop of solution is not the same for each scan.

$$\left|\chi^{(3)}_{1111,sol}\right| \propto \frac{n_{3\omega,sol}}{n^{3/2}_{\omega,sol}} \frac{1}{\sqrt{T_{3\omega,sol}T^3_{\omega,sol}}} \frac{1}{\left|J_{3\omega,sol}(\Delta k_{sol};-L_{sol};0)\right|} \sqrt{S_{3\omega}} \quad (24)$$

The sol subscript refers to colloidal solution. No absorption corrections have been performed since only the signal at the solution/air interface is considered. Moreover, since the solutions are much diluted, one can consider that their refractive index is the same than the one of water. The only parameters which change from one sample to another are $S_{3\omega}$ and $J_{3\omega,sol}$, since the thickness of the drops is not the same. For each solution, the magnitude of the third-harmonic signal at the solution/air interface has been measured and the third-harmonic interaction length has been calculated. The variation of the third-order susceptibility of the CdS@Ag$_n$ colloidal solution relative to the colloidal CdS solution has been then determined, reduced to the same concentration (*i.e.* 10^{-4} mol.L^{-1}):

$$\frac{\Delta\chi^{(3)}}{\chi^{(3)}} = \frac{\chi^{(3)}_{CdS@Ag_n} - \chi^{(3)}_{CdS}}{\chi^{(3)}_{CdS}} \times 100 \approx 96\% \quad (21)$$

It appears that the CdS@Ag$_n$ colloidal solution presents third-order susceptibility almost twice much higher than the CdS one's. An increase of the nonlinearity of CdS in close vicinity with metallic silver has been already proposed [27]. For a clear understanding of the silver metallic island contribution on CdS nonlinear optical response, a more systematic study is necessary including the response of metallic particles alone.

V. CONCLUSION

THG microscopy appears to be a powerful tool in electronic nonlinear optical properties characterization. This technique allows measurements on bulk materials as well as on solutions or thin films. In theory, this technique is able to supply absolute measurements. In practice, it is very difficult to know precisely all the experimental parameters (effective third-harmonic power, fundamental power at the sample, pulse duration at the sample, collection and detection efficiencies) which is why this technique is used to provide relative measurements. An issue to perform absolute measurements would be to have a very well-known reference value of the electronic third-order susceptibility, such as fused silica. Unfortunately, such measurement with a low uncertainty has not been achieved with satisfaction.

ACKNOWLEDGEMENTS

This work was supported by the Centre National de la Recherche Scientifique, the Agence Nationale de la Recherche (ANR-05-BLAN-0212-01), the National Research Laboratory Program (M1-0203-00-0082) through the Ministry of Science and Technology (MOST) of Korea, the Brain Korea 21 project of the Ministry of Education, the International Coopeeration Research Program (M6-0520-00-0116) of MOST and the French Embassy in Seoul. The authors want to thank Arnaud Brocas, Eddie Maillard, Touati Douare, Sébastien Cassagnère and William Benharbone for their technical assistance on the construction of the THG microscopes as well as Artem Malakho and Frédéric Rocco for the preparation of the poled glasses and the colloidal solutions, respectively.

*Corresponding author: a.royon@cpmoh.u-bordeaux1.fr

REFERENCES

[1] P. S. Banks, M. D. Feit, and M. D. Perry, "High intensity direct third harmonic generation in BBO," in *Nonlinear Optics '98: Materials, Fundamentals, and Applications Topical Meeting*, Kauai, USA, 1998, pp. 268-270.

[2] D. Taverner, P. Britton, P. G. R. Smith, D. J. Richardson, G. W. Ross, and D. C. Hanna, "Highly efficient second-harmonic and sum-frequency generation of nanosecond pulses in a cascading erbium-doped fiber: periodically poled lithium niobate source," *Optics*

Letters, vol. 23, pp. 162-164 (1998).

[3] B. Buchalter and G. R. Meredith, "Third-order optical susceptibility of glasses determined by third harmonic generation," *Applied Optics*, vol. 21, pp. 3221-3224 (1982).

[4] H. Nasu, K. Kubodera, M. Kobayashi, M. Nakamura, and K. Kamiya, "Third-Harmonic Generation from Some Chalcogenide Glasses," *Journal of the American Ceramic Society*, vol. 73, pp. 1794-1796 (1990).

[5] S. H. Kim, T. Yoko, and S. Sakka, "Nonlinear Optical Properties of TeO_2-Based Glasses: La_2O_3-TeO_2 Binary Glasses," *Journal of the American Ceramic Society*, vol. 76, pp. 865-869 (1992).

[6] U. Gubler and C. Bosshard, "Optical third-harmonic generation of fused silica in gas atmosphere: Absolute value of the third-order nonlinear susceptibility $x^{(3)}$," *Physical Review B*, vol. 61, pp. 702-710 (2000).

[7] T. Y. F. Tsang, "Optical third harmonic generation at interfaces," *Physical Review A*, vol. 52, pp. 4116-4126 (1995).

[8] Y. Barad, H. Eisenberg, M. Horowitz, and Y. Silberberg, "Nonlinear scanning laser microscopy by third harmonic generation," *Applied Physics Letters*, vol. 70, pp. 922-924 (1997).

[9] L. Canioni, S. Rivet, L. Sarger, R. Barille, P. Vacher, and P. Voisin, "Imaging of Ca^{2+} intracellular dynamics with a third-harmonic generation microscope," *Optics Letters*, vol. 26, pp. 515-517 (2001).

[10] D. Yelin and Y. Silberberg, "Laser scanning third-harmonic-generation-microscopy in biology," *Optics Express*, vol. 5, pp. 169-175 (1999).

[11] J. A. Squier, M. Muller, G. J. Brakenhoff, and K. R. Wilson, "Third harmonic generation microscopy," *Optics Express*, vol. 3, pp. 315-324 (1998).

[12] D. Debarre, W. Supatto, A. M. Pena, A. Fabre, T. Tordjmann, L. Combettes, M. C. Schanne-Klein, and E. Beaurepaire, "Imaging lipid bodies in cell and tissues using third-harmonic generation microscopy," *Nature Methods*, vol. 3, pp. 47-53 (2006).

[13] R. Barille, L. Canioni, L. Sarger, and G. Rivoire, "Nonlinearity measurements of thin films by third-harmonic-generation microscopy," *Physical Review E*, vol. 66, pp. 067602-067605 (2002).

[14] J. M. Schins, T. Schrama, J. Squier, G. J. Brakenhoff, and M. Muller, "Determination of materials properties by use of third-harmonic generation microscopy," *Journal of Optical Society of America B*, vol. 19, pp. 1627-1634 (2002).

[15] V. Shcheslavskiy, G. Petrov, and V. V. Yakovlev, "Nonlinear optical susceptibility measurements of solutions using third-harmonic generation on the interface," *Applied Physics Letters*, vol. 82, pp. 3982-3984 (2003).

[16] P. N. Butcher and D. Cotter, *The Elements of Nonlinear Optics* (Cambridge University Press, Cambridge, UK, 1990), p. 225 and appendix 10.

[17] R. W. Boyd, *Nonlinear Optics* (Academic Press, New York, USA, 2003), pp. 90-99.

[18] A. Brocas, *Microscopies non-linéaires: Analyses et Instrumentations* (Thesis, University of Bordeaux 1, France, 2005).

[19] D. Oron, E. Tal, and Y. Silberberg, "Depth-resolved multiphoton polarization microscopy by third-harmonic generation," *Optics Letters*, vol. 28, pp. 2315-2317 (2003).

[20] D. Oron, D. Yelin, E. Tal, S. Raz, R. Fachima, and Y. Silberberg, "Depth-resolved structural imaging by third-harmonic generation microscopy," *Journal of Structural Biology*, vol. 147, pp. 3-11 (2004).

[21] T. Cardinal, E. Fargin, G. Le Flem, M. Couzi, L. Canioni, P. Segonds, L. Sarger, A. Ducasse, and F. Adamietz, "Nonlinear optical properties of some niobium (V) oxide glasses," *European Journal of Solid State and Inorganic Chemistry*, vol. 33, pp. 597-605 (1996).

[22] T. Cardinal, E. Fargin, G. Le Flem, and S. Leboiteux, "Correlations between structural properties of Nb_2O_5-$NaPO_3$-$Na_2B_4O_7$ glasses and non-linear optical activities," *Journal of Non-Crystalline Solids*, vol. 222, pp. 228-234 (1997).

[23] A. Malakho, M. Dussauze, E. Fargin, B. Lazoryak, V. Rodriguez, and F. Adamietz, "Crystallization and second harmonic generation in thermally poled niobium borophosphate glasses," *Journal of Solid State Chemistry*, vol. 178, pp. 1888-1897 (2005).

[24] A. Zoubir, M. Richardson, L. Canioni, A. Brocas, and L. Sarger, "Optical properties of infrared femtosecond laser-modified fused silica and application to waveguide fabrication", *Journal of Optical Society of America B*, vol. 22, pp. 2138-2143 (2005).

[25] D. Blomer, A. Szameit, F. Dreisow, T. Schreiber, S. Nolte, and A. Tunnermann, "Nonlinear refractive-index of fs-laser-written waveguides in fused silica," *Optics Express*, vol. 14, pp. 2151-2157 (2006).

[26] F. Rocco, A. K. Jain, M. Treguer, T. Cardinal, S. Yotte, P. Le Coustumer, C. Y. Lee, S. H. Park, and J. G. Choi, "Optical response of silver coatings on CdS colloids," *Chemical Physics Letters*, vol. 394, pp. 324-328 (2004).

[27] N. Kalyaniwalla, J. W. Haus, R. Inguva, and M. H. Birnboim, "Intrinsic optical bistability for coated spheroidal particles," *Physical Review A*, vol. 42, pp. 5613-5621 (1990).